MPC for optimal dispatch of an AC-linked hybrid PV/wind/biomass/H_2 system incorporating demand response.

César Y. Acevedo-Arenas[1], Antonio Correcher[2], Carlos Sánchez-Díaz[3], Eduardo Ariza[4], David Alfonso[3], Carlos Vargas[3], Johann F. Petit-Suárez[5]

[1] GIRES, Universidad Autónoma de Bucaramanga, Bucaramanga, Colombia.

[2] Ai2, Universitat Politècnica de València, Valencia, Spain.

[3] IUIIE, Universitat Politècnica de València, Valencia, Spain.

[4] Corporación Universitaria Comfacauca, Popayán, Colombia.

[5] GISEL, Universidad Industrial de Santander, Bucaramanga, Colombia.

Summary.

A Model Predictive Control (MPC) strategy based on the Evolutionary Algorithms (EA) is proposed for the optimal dispatch of renewable generation units and demand response in a grid-tied hybrid system. The generating system is based on the experimental setup installed in a Distributed Energy Resources Laboratory (LabDER), which includes an AC micro-grid with small scale PV/Wind/Biomass systems. Energy storage is by lead-acid batteries and an H2 system (electrolyzer, H2 cylinders and Fuel Cell). The energy demand is residential in nature, consisting of a base load plus others that can be disconnected or moved to other times of the day within a demand response program. Based on the experimental data from each of the LabDER renewable generation and storage systems, a micro-grid operating model was developed in MATLAB© to simulate energy flows and their interaction with the grid. The proposed optimization algorithm seeks the minimum hourly cost of the energy consumed by the demand and the maximum use of renewable resources, using the minimum computational resources. The simulation results of the experimental micro-grid are given with seasonal data and the benefits of using the algorithm are pointed out.

Keywords.

Model Predictive Control, Genetic Algorithm, Hybrid energy systems, Micro-grids

1. Introduction.

Increasing awareness of the impact of conventional energy generating systems on sustainability, the frequent incorporation of public policies for integrating renewable sources in the energy generation matrix, and the development of increasingly affordable small-scale distributed generation technology [1] are all factors that have led to the growth in the use of small hybrid generating systems for residential use. These systems use renewable energies to reduce the local demand on the public grid and can stay connected to act as a backup when renewable energy is generated. The grid can also be used to maintain reference voltages and frequency and any power surplus produced by the micro-grid can be sold off. The development of regulatory schemes in the small-scale consumer market, which allow for hourly price differentiation, gives the option of a hybrid generating system to small residential consumers and opens up the possibility of importing or exporting energy from/to the grid according to hourly prices and the energy resources available.

In this type of project, the capital, operating, maintenance and replacements costs, in relation to the power consumed, should result in a lower price than the electrical energy tariff of a final consumer. These benefits must be maintained throughout the lifetime of the installation in order to recover the investment and to consume the lowest amount of energy from the grid [2].

As neither solar nor wind energy are dispatchable resources, one or more storage systems are necessary to provide a reliable energy system, and since a wide range of different elements may be involved, these systems must be optimized in order to achieve technical and economic feasibility.

Considering the small margin between the levelized cost of electricity – LCOE and the hourly final consumer grid tariff, the energy supply and demand in the micro-grid must be carefully managed. This margin is the factor which determines whether the power supply is bought from the grid or consumed from the micro-grid's renewable resources.

A number of studies have been published recently on the optimization of micro-grid systems [3] or hybrid energy generation systems. In [4], different analysis software tools for hybrid systems are described. However, in the literature, optimization is usually achieved by considering the dimensioning of the PV-Wind-Battery off-grid hybrid system [5], dimensioning plus a hydrogen storage system [6], genetic algorithms [7,8] or comparing the new algorithms with classical techniques [9,10]. The optimization parameters do not always reduce costs, but may deal with the maximum allowable loss of supply probability LPSP [11] or even social-environmental aspects as well as technical-economic aspects [12]. In [13,14], genetic algorithms are used to dimension an isolated system using hydrogen for energy storage.

However, genetic algorithms are not only used in isolated systems to optimize the design. In [15] the Particle Swarm Optimization algorithm is used to dimension a tie-grid hybrid system including different renewable energy sources (PV, Wind, Solar Heat, Biomass).

Apart from dimensioning, these algorithms have also been used to control energy flow in tie-grid hybrid systems. In some cases these are simple hybrid systems composed of PV and batteries [16], while others include wind energy and hydrogen [17] or simply demand response [18]. The flexibility of genetic algorithms thus makes it possible to achieve a number of different objectives, including economic and environmental, using a hybrid algorithm in a tie-grid system consisting of photovoltaics, batteries and a fuel cell powered by natural gas [19]. Daily operation is a simple tie-grid hybrid system (PV, wind, batteries and diesel) that is cost optimized by the predictive control algorithms in [20] to improve the system behavior when under the conventional “load following” strategy. The improvements have been reported to reach 36%.

This paper proposes a supervisory control that schedules daily inputs to be implemented in the system. When possible, the controller decides the power to be delivered from the generation subsystems (i.e. biomass and fuel cell), while also programming how the loads specified in the demand response program will be met.

In order to decide the inputs (power generation and demand response program loads), the controller simulates the system to predict the consequences of these actions and measure the system performance by an index including the overall cost. The best control action will thus be the one that achieves the best score. This control method is known as the model predictive control (MPC).

The MPC optimization procedure is closely related to the definition of the model to be simulated [21]. Although conventional optimization techniques (linear programming) can be used to optimize the controller, these methods are not effective on complex models. In these cases [22], metaheuristic optimization can be used to search for the optimal solution. In [23] a MPC approach is used to optimize the management of a hybrid PV-Wind-Batteries system. The goal is to achieve high profitability by selling energy from renewable sources to the grid. The MPC algorithm is used to forecast the price of the energy hour by hour and to decide if the energy is stored or sold. In [24] a MPC algorithm is used to optimize the hydrogen production via anaerobic fermentation of glucose in a hybrid system PV-Wind-Hydrogen.

This study used a metaheuristic optimization procedure based on an Evolutionary Algorithm (EA). EAs are algorithms that simulate the biological evolution of a species so that each proposed solution evolves and improves on a previous set of possible solutions [25]. Several modern EAs can be used to search for the best solution of the MPC problem [26,27]. The particle swarm optimization (PSO) algorithm used in the present study has been shown to perform well in identification applications [28].

The micro-grid is based on the Distributed Energy Resources Laboratory (LabDER, IUIIE, *Universitat Politècnica de València*) generation and energy storage equipment. The design of this existing generating system is not described here. The proposed tool uses the forecast weather variables and hourly energy prices to the final consumer to program the next day’s dispatchable generation and switchable loads.

The paper is organized as follows: Section 2 describes the overall system and how the mathematical model of each generating element was obtained. The energy management system is described in Section 3. Section 4 explains the design of the genetic algorithm and specifies the scenarios to be simulated. Section 5 gives the results obtained from the different client configurations (3, 5 or 7 households), while our conclusions are given in Section 6.

2. System components, characteristics and models.

The LabDER's experimental micro-grid has four solar, wind, biomass and hydrogen renewable energy systems, in addition to batteries, hydrogen bottles and dry biomass fuel. This hybrid generating system can operate in isolation, interconnected to feed a programmable load or deliver power to the grid. It also has a Supervisory Control and Data Acquisition (SCADA) management and control system to monitor the available energy resources and generation mix, as well as directing energy in any direction from or to the storage systems, to the load or the public grid. Figure 1 shows a diagram of the LabDER system, with the current configuration in terms of components and connections. A more detailed description of this micro-grid can be found in [29,30].

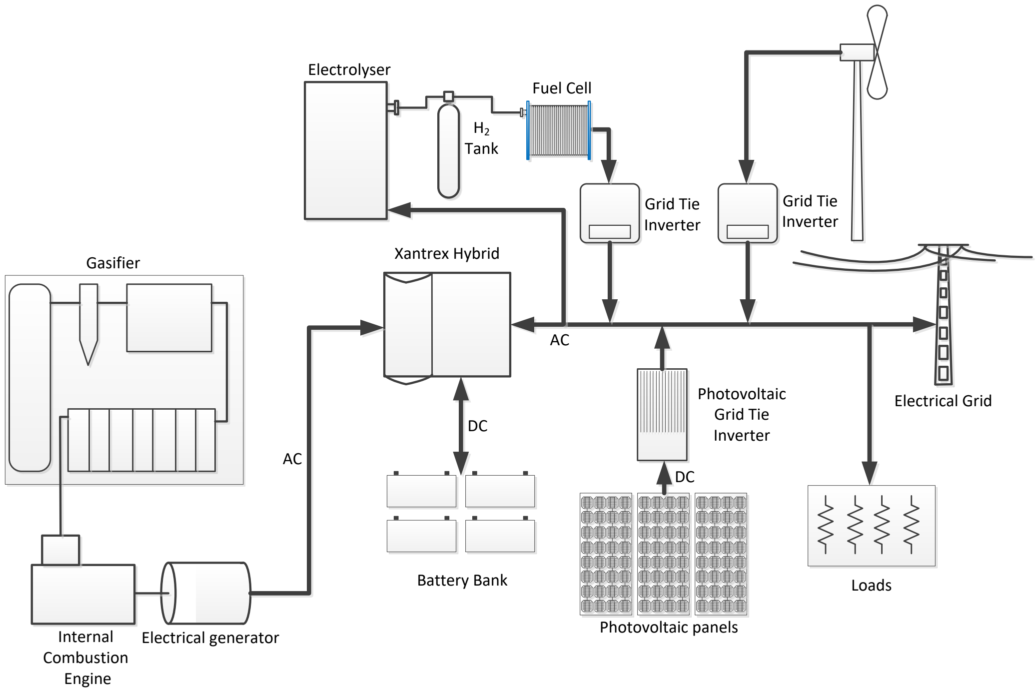

FIGURE 1 Diagram of LabDER configuration.

An operating model was developed to simulate the integrated energy balance of a real interconnected micro-grid for residential consumers. The components of the experimental micro-grid, its characteristics, modeling, simulation and operating data are described below.

2.1 Photovoltaic system.

The PV System consists of 11 modules of three different specifications. All modules are connected in series for academic and experimental purposes. The PV array is composed of 4 Zhejiang Wanxiang Solar WSX180 modules of Si Monocrystalline (180 Wp), 5 Rec Solar 230AE Modules of Si Polycrystalline (230 Wp) and 2 USL Photovoltaics USP145 Modules of Si Polycrystalline (145 Wp). Therefore, the total installed peak power is 2160 W. This energy flows to a Xantrex GT 2.5-DE (2.5 kW) tie inverter connected to a common single-phase AC bus.

The mathematical model of each PV module was developed from its equivalent circuit, as shown in Figure 2. The model parameters from A. Bellini et al. [31] together with the modifications proposed by A. Hadj Arab et al. [32] and M. Villalba et al. [33] were used in (1) to establish the parameters of the equivalent circuit.

$$I_P = I_{SC}\left[1 - C_1\left(e^{\left(\frac{V_P}{C_2 \cdot V_{OC}}\right)} - 1\right)\right] \quad (1)$$

where

$$C_1 = \left(1 - \frac{I_{MPPS}}{I_{SCS}}\right) \cdot e^{\left(\frac{-V_{MPPS}}{C_2 \cdot V_{OCS}}\right)} \quad and, \quad C_2 = \frac{\left(\frac{V_{MPPS}}{V_{OCS}} - 1\right)}{\ln\left(1 - \frac{I_{MPPS}}{I_{SCS}}\right)} \quad (2)$$

Coefficients C_1 and C_2 depend on parameters defined in standard conditions of irradiance and temperature (G_S=1000W/m^2 and T_S=25°C) such as: short circuit current I_{SCS}, open circuit voltage V_{OCS}, maximum power point voltage V_{MPPS} and maximum power point current I_{MPPS}. Appendix 1 explains how the parameters were calculated in other operational conditions.

The equivalent circuits of each module were connected in series and the total voltage and current of the photovoltaic array V_{array} and I_{array} were determined. The power of the PV system is calculated by Eq.(3).

$$P_{PV} = V_{array} \cdot I_{array} \cdot \eta_{inv} \quad (3)$$

Figure 2 shows the equivalent circuit of a PV device and figure 3 compares the results obtained from the LabDER tests and those of the MATLAB© model. A root-mean-square error (RMSE) of 72.45W was obtained between the set of measurements and its corresponding result in the MATLAB© model.

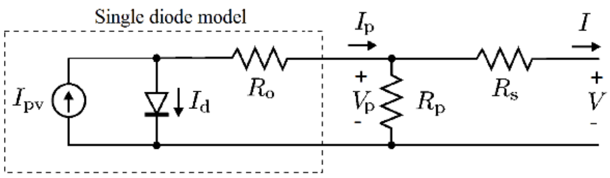

FIGURE 2 Single-diode model - Equivalent circuit of a practical PV device.

Table 1 shows the parameters in each of the three solar module specifications and the result of the coefficients C_1 and C_2.

TABLE 1 Characteristics and parameters of the PV array modules.

	Zhejiang Wanxiang Solar	Rec Solar	USL Photovoltaics
Model	WSX180	230AE	USP 145
Number of Modules	4	5	2
Type	Monocrystalline	Polycrystalline	Polycrystalline
Maximum Power	180 W	230 W	145 W
Maximum Power Voltage	35.36 V	29.0 V	33.5 V
Maximum Power Current	4.79 A	8.0 A	4.57 A
Open Circuit Voltage	43.88 V	36.9 V	42.7 A
Short Circuit Current	5.18 A	8.6 A	5.03 A
C_1	1.64029 x10^{-6}	1.83985 x10^{-7}	1.50857x10^{-5}
C_2	0.07507	0.06448	0.09007

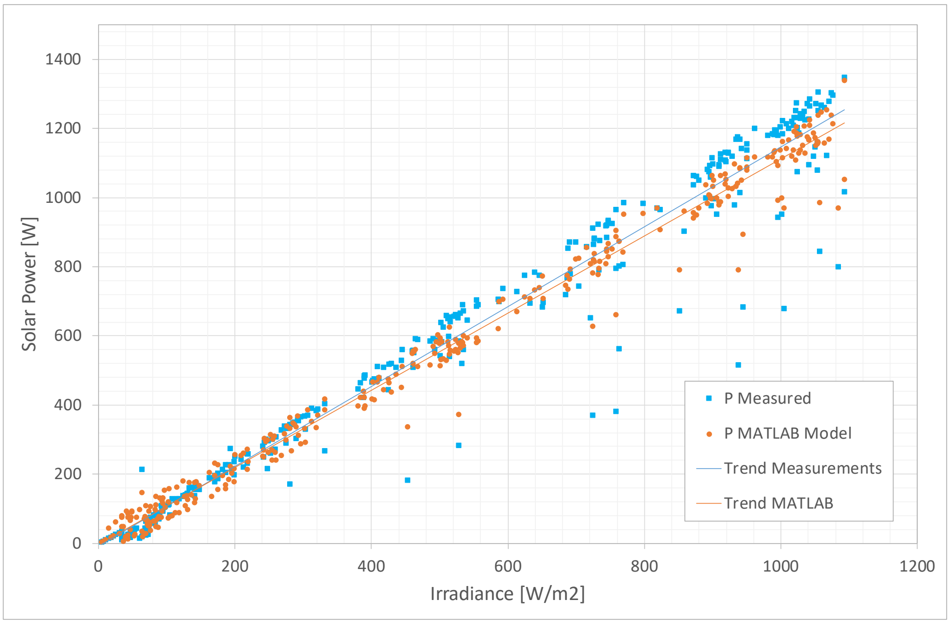

FIGURE 3 Comparison between the Power from the PV Array obtained by MATLAB model and real data.

2.2 Wind system.

The wind system consists of an Anelion SW 3.5-GT 3-bladed wind turbine with a rotor diameter of 3.5 m and a nominal capacity of 4000 W and a tower height of 21 m. The AC voltage (up to 400 Vrms) is connected to a rectifier that delivers a DC signal to a Grid-tied SMA Windy Boy WB2500 inverter connected to the single-phase AC bus.

For modeling purposes, the power curve provided by the wind turbine manufacturer, applying Hellmann's exponential law, was used to correct the wind speed at the wind turbine hub as expressed in Eq.(4).

$$v = v_0 \left(\frac{H}{H_0} \right)^{\gamma} \tag{4}$$

where v is the speed to the height H, $v_0$is the speed to the height H_0 (frequently referred to as 10-m) and γ is the friction coefficient or Hellman exponent.
A curve adjustment was made using the “pchip” function (Piecewise Cubic Hermite Interpolating Polynomial) as proposed by Lydia et al. [34]. A power adjustment was also applied due to the effect of air density at different heights. The expression for output power of a wind turbine can be related to wind speed by Eq.(5).

$$P_W = \begin{cases} 0, & v < vci \quad or \quad v \geq vco \\ P_{W-adj} \cdot CF_{dens-temp} \cdot \eta_{inv}, & vci \leq v < vco \end{cases} \tag{5}$$

where *vci*, *vco* and *v* are cut-in, cut-off and wind speed adjusted for Hellmann´s law, respectively. $P_{W\text{-}adj}$ is the final wind power output in the common single-phase AC bus obtained by the pchip MATLAB© function and adjusted to wind speed *v*, $C_{Fdens\text{-}temp}$ is a correction factor for density and temperature effect and η_{inv} is the inverter efficiency. Table 2 shows the wind system parameters.

TABLE 2 Wind Energy System – Turbine and grid-tie inverter features.

Anelion Wind Turbine	
Model	SW 3.5-GT
Rated Power Output	4 kW
Type	3 blades, horizontal axis
Generator	Direct Drive PMSG
Swept Area	9.62 m^2
Rated Wind Speed	12 m/s
Start-up Wind Speed	3.5 m/s
Survival Wind Speed	17,5 m/s
Voltage/Phase	400 Vrms
Current/Phase	20 Arms
SMA Grid-tie Inverter	
Model	Windy Boy WB2500
Input Voltage Range	224 – 600 V_{DC}
Maximum Input Power	2700 W
Maximum Input Current	12 A_{DC}
Nominal Output Peak Power	2500 W
Nominal Output Current	9.6 Arms
Operating Range Grid Voltage	180 – 265 V_{AC}
Operating Range Grid Frecuency	45.5 – 54.5 Hz

Figure 4 compares the results obtained from the LabDER tests and the simulations of the MATLAB© model. The real data was different from the manufacturer's curve and our model fitted the real behavior instead of the nominal behavior in the datasheet. The RMSE obtained between the set of measurements and its corresponding result in the MATLAB© model was 140.5W.

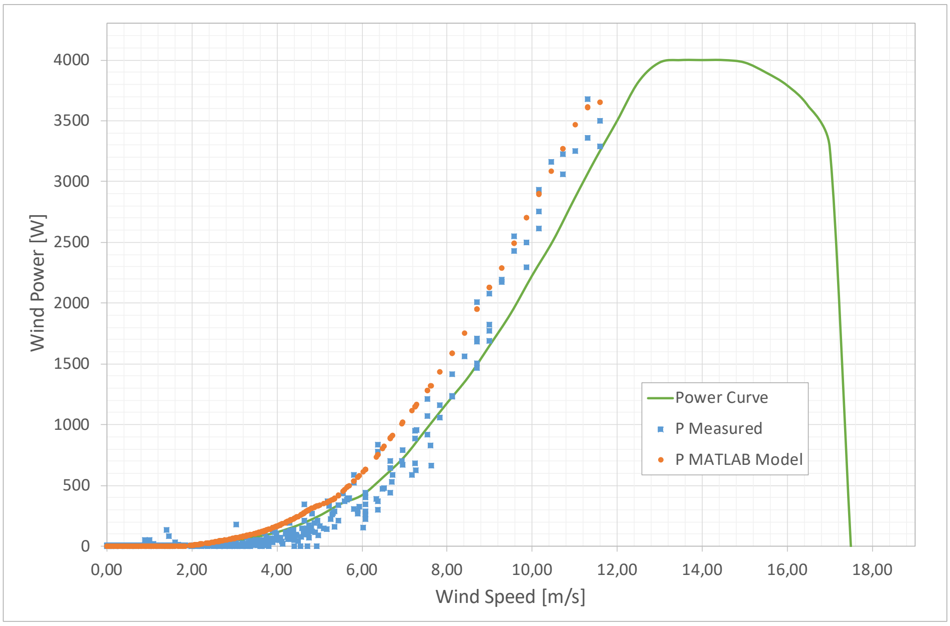

FIGURE 4 Comparison of the power from the wind turbine obtained by MATLAB model and real operation (continuous line shows the manufacturer curve).

2.3 Biomass system.

This system consists of a gasification plant and a generator set connected to the common single-phase AC bus with a maximum power of 10 kW, producing a synthesis gas at a flow of 27 to 33 Nm3/h which is burned in an internal combustion engine. To optimize operations its daily generation schedule in a real application must be planne4d. The FG Wilson UG14P1 generating set consists of a 1.8 litre HM natural gas engine, adapted to burn syngas and a Leroy Somer LUA1014NX 10 kW synchronous generator. This adaptation changes the performance of the generating system to an electrical generating capacity of 8.7 kW. Table 3 summarizes the main parameters of the biomass generation system.

TABLE 3 Gasification power plant features.

Biomass Gasification Reactor	
Type	Bubbling fluidized bed
Biomass reactor dimensions	Diameter: 106 mm, Height: 155 mm
Fuel type	Wood chips (10 - 15 mm maximum length)
	Pellets (diameter 6 mm, 15 - 25 mm length)
Biomass hopper capacity	237.l (up to 166 kg of biomass)
Biomass input (@ 10%	6 – 13 kg/h
	30 - 60 kWt (referred to higher heating value)
Syngas production	13 – 33 Nm3/h
Syngas higher heating value	5 – 5.8 MJ/Nm3
Global efficiency	14 – 20%
FG Wilson Generator Set	
Model	UG14p1
Cylinder capacity	1.8 L
Engine velocity	1500 rpm
Compression ratio	8.5:1
Fuel Consumption	2475 m3/h (Gas Natural)
	7.5 kg/h (Syngas)
Rated Electric Power	10 kW (Gas Natural)
	8.7 kW (Syngas)
Voltage and Frequency	220/240 V_{AC} & 50 Hz

The energy balance equations of the model can be entered in the MATLAB model based on Vargas's proposal [35] and applied to the economic analysis by Montouri [36] from efficiency curves. The curve fit was based on the experimental results (Eq. (6)).

$$Q_{Bio} = -21.577\times10^{-12} P_{Gasif}^{3} + 223.972\times10^{-9} P_{Gasif}^{2} + 339.382\times10^{-6} P_{Gasif} + 4.8264 \quad (6)$$

where Q_{Bio} is the biomass flow into the gasifier and P_{Gasif} is the active power in the common single-phase AC bus.

Since the gasifier produces dispatchable energy, the input argument for the function is in this case the power on the single-phase AC side. Figure 5 shows the comparison between the results obtained from the LabDER tests and the MATLAB© simulations. As expected, the simulated data fitted perfectly with the experimental data; in this case, the RMSE obtained between the set of measurements and its corresponding result in the MATLAB© model was 0.28 kg/h.

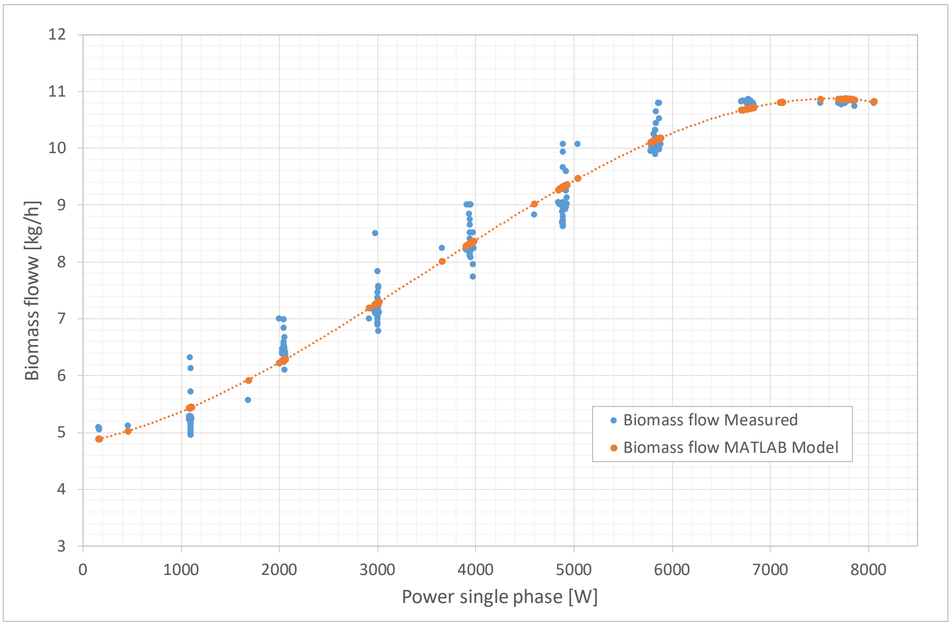

FIGURE 5 Comparison between the Power from the Gasifier obtained by MATLAB model and real operation.

2.4 Hydrogen system

This system consists of an electrolyzer, a compressor, a bottle of H_2 and a PEM (Proton Exchange Membrane) fuel cell. Its main purpose is to absorb excess energy and then store it in the form of hydrogen.

An Erre Due G2.0 electrolyzer is used to produce H_2 with a maximum production capacity of 1.33 Nm3/h at a pressure of 4 bar. For its operation, it requires a three-phase power supply with a nominal electrical power of 7.2 kW. At present, the electrolyzer is connected to the grid, but for the purposes of the hydrogen system described above, a single-phase AC-DC-AC three-phase converter is proposed in the model to allow excess energy to be used in the common single-phase AC bus. Hydrogen is compressed to 200 bar in the bottle. Table 4 shows the principal characteristics of the hydrogen energy system.

TABLE 4. Hydrogen Energy System – Electrolyzer and Fuel Cell Stack.

Erre Due Electrolyzer	
Model	ED-G2.0
Rated Power	7,2 kW
Electric Power Suply	3x400 V + N & 50 Hz
Hydrogen Production	1.33 Nm^3/h
Oxygen Production	0.66 Nm^3/h
Deionized Water Consumption	1.2 l/h
Hydrogen Purity	99.3 – 99.8%
Hydrogen Purity	98.5 – 99.5%
Ballard Fuel Cell Stack	
Model	Nexa 1200
Type	PEM
Rated Power	1200 W
Rated Current	52 A_{DC}

Output Voltage (unregulated)	20 – 36 V_{DC}
Operating Temperature	5 – 35°C
Hydrogen Quality	4.0 (99.99 % or better)
Hydrogen Consumption	15 Slpm (at rated output)
Air Consumption	335 m^3/h (at rated output, 30 °C ambient temperature)

For the MATLAB© simulation a function was developed from the curve fit with experimental data using Smoothing Spline, where *f(x)* is a piecewise polynomial computed from $p=4.7396674\times10^{-9}$ as a smoothing parameter. Figure 6 (a) shows the hydrogen production obtained from the LabDER tests and the MATLAB© simulations. The RMSE between the set of measurements and its corresponding result in the MATLAB© model was 26.91 NL/h

The fuel cell system used in LabDER is a Ballard Nexa 1.2 kW commercial stack producing up to 1200 W of unregulated DC power from a hydrogen and oxygen supply. The fuel cell is electrically connected to the common single-phase AC bus via a 1200 W pure sine wave inverter specifically designed for this application. For the MATLAB© model a curve fit was performed with the experimental data (Eq. (7)).

$$QH2 = 42.199\times10^{-9} P_{FCdc}^{2} + 136.454\times10^{-6} P_{FCdc} + 1.906\times10^{-3} \tag{7}$$

Where *QH2* is the Hydrogen Flow from the bottle to the fuel cell and P_{FCdc} is the power of the stack on the DC side. Figure 6 (b) compares the experimental results with the MATLAB© model [37, 38]. The RMSE obtained between the set of measurements and its corresponding result in the MATLAB© model was 18.47 NL/h.

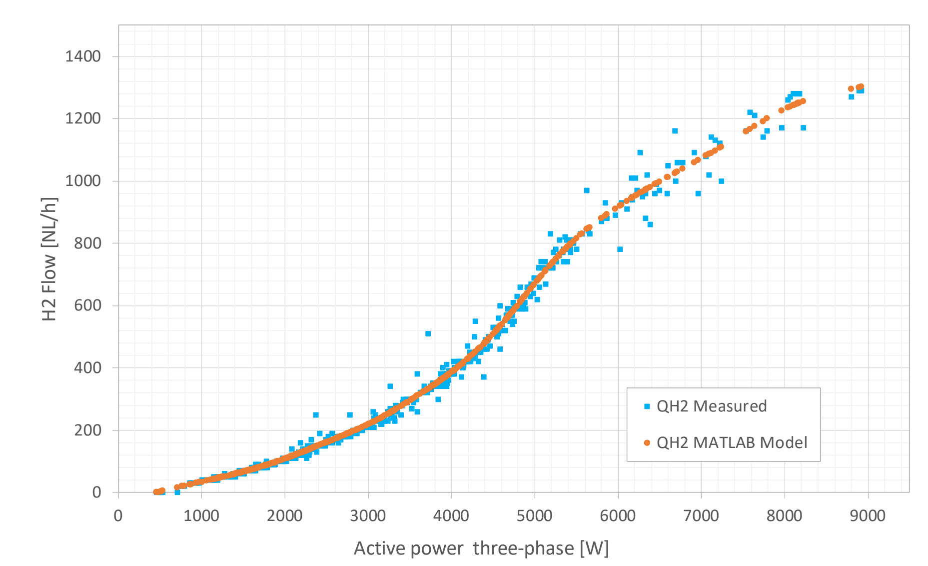

a) Electrolyser

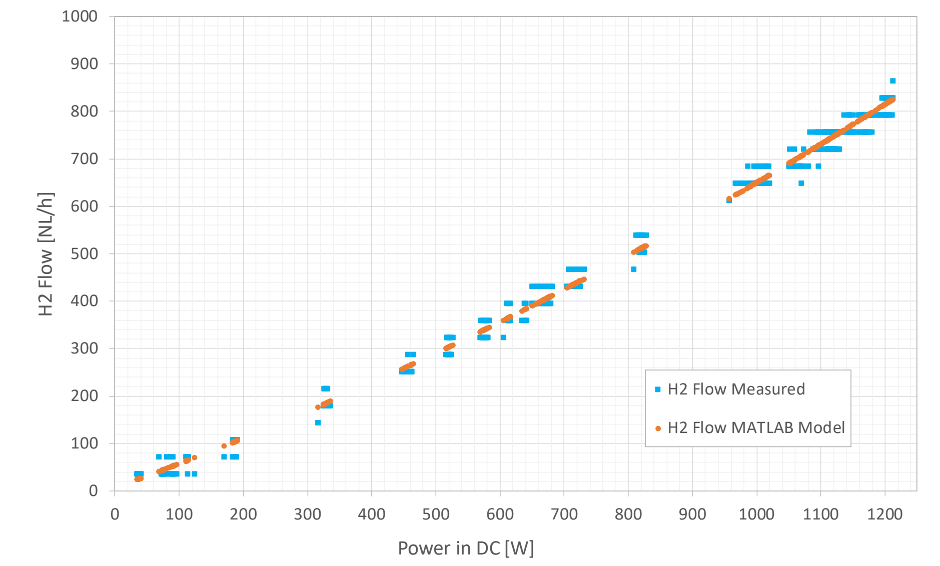

b) Fuel Cell

FIGURE 6 Comparison between the hydrogen production in the electrolyzer (a) and hydrogen consumed in the fuel cell (b) from real operational data and the MATLAB model.

2.5 Batteries.

The other storage system modeled was the battery bank, which is composed of four Saclima Power 250 12V 250 Ah C100 lead-acid Monoblock batteries connected in series, which supply a voltage of 48 VDC with a nominal capacity of 12000 Wh. The battery bank is connected to a XANTREX XW4548 inverter-charger and central micro grid controller, which allows maximum battery discharge of up to 40% of the nominal capacity to extend its service life.

The model developed in MATLAB© was based on the energy balance. To adjust the models, a test was carried out in which the batteries were charged by connecting them to the grid and discharged by controlled demand. Figure 7 shows the data from this experiment. The difference in the results is due to the data measurement: directly on the battery side in the real operation and in the common single-phase AC bus in the MATLAB model.

If the difference between the generated energy a demand is positive and the batteries have already been charged to 100% (State of Charge - SOC in the maximum value), this energy would be used to produce hydrogen in the electrolyzer, and any further excess is delivered to the electrical grid. If the difference is negative, the battery delivers its power to meet demand until its state of charge - SOC is the minimum set point; if the deficit persists, power will be imported from the grid. The equation (8) shows the above process, performing the power flow balance in the common single-phase AC bus.

$$P_{BAT} = \begin{cases} 0 \quad if, \quad SOC = SOC_{MAX} \vee SOC < SOC_{MIN} \\ (P_{PV} + P_W + P_{Gasif}) - P_{LOAD} \quad if, \quad SOC_{MIN} \le SOC < SOC_{MAX} \end{cases} \tag{8}$$

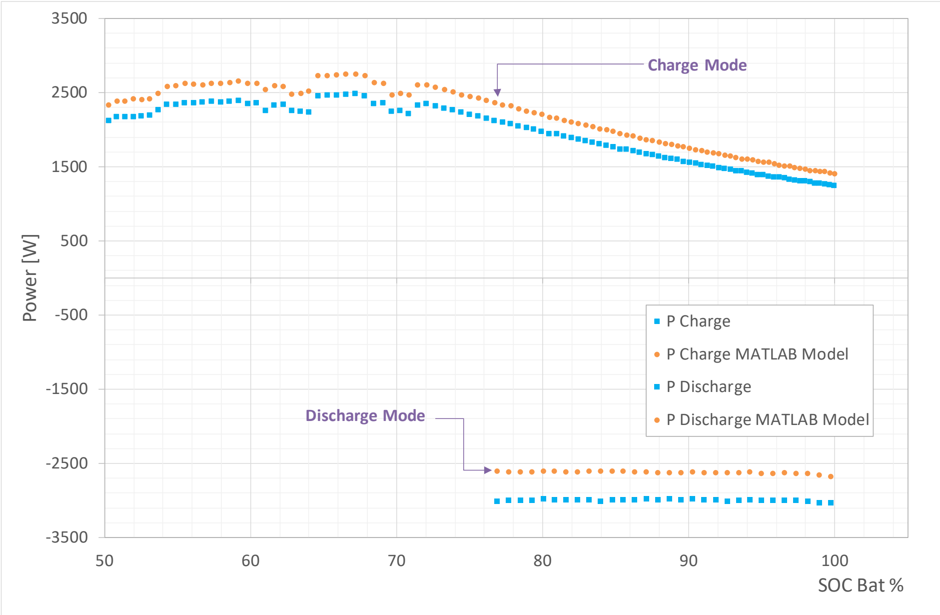

FIGURE 7 Comparison of real battery operation and the MATLAB model.

2.5 Loads.

To model the load in the experimental micro-grid, a demand behavior was proposed as a function of a typical residential curve, which passes through 3 seasonal periods in the year: Winter, Summer and Spring-Autumn. Figure 8, shows the base demand curve of a household in "per unit" values (p.u.), from which it is possible to vary the maximum demand, add the number of households, consider randomness and take into account the effect of additional loads which are enrolled in a demand response program.

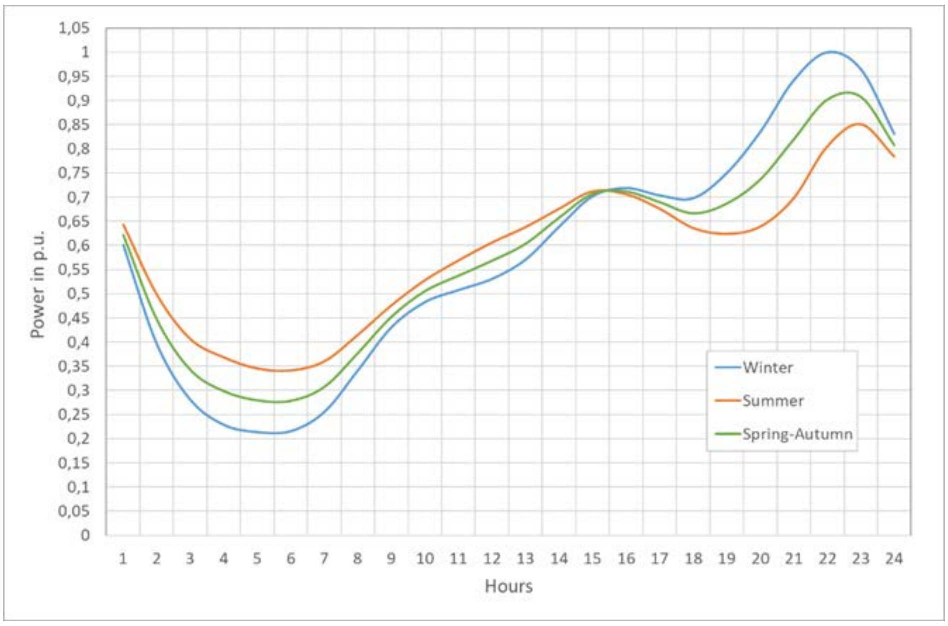

FIGURE 8 Base load power (per unit)

The total power consumed by the demand can be expressed in Eq.(9) for each hour of the day.

$$P_{LOAD} = (P_{pu} \cdot D_{MAX} \cdot N_H \cdot R) + P_{DR} = P_{BASE} + P_{DR} \quad (9)$$

P_{pu} is the hourly demand of one household in per unit, D_{MAX} is the maximum demand of one household, N_H is the number of households considered (from 1 to 20), R is a randomness factor calculated by Eq.(10) and P_{DR} is the sum of the power of the loads enrolled in the demand response program, which can be disconnected or moved to another time during the day.

$$R = \frac{(100 + V_D) - ((100 + V_D) - (100 - V_D)) * rand}{100} \quad (10)$$

Where V_D is the percentage of the desired demand variation interval (usually between 0% and 15%) and *rand* is a random number generated by the computer between 0 and 1.

Additional loads associated with a demand response program in 5 houses were considered. Loads were assumed to be part of the demand response program in 5 homes, plus a communal water pumping system to an overhead tank, whose power varies according to the number of homes (for 5 households the power is 2 HP for 2 hours of operation). Residential energy consumption habits of household users was taken into account to define the initial response demand program. One of the controller task is to locate these loads during the day in an optimal position under criteria of cost and energy availability. The loads registered for each household are shown in Table 5.

TABLE 5 Characteristics of dispatchable loads.

Household/Load	Power [W]	Operating Time [h]	Initial Daily Timing [h]
1/Dishwasher	600	3	9:00 to 11:59
1/Charger electric vehicle	3375	3	22:00 to 24:59
2/ Pool treatment plant	2500	3	14:00 to 16:59
3/ Pool treatment plant	2000	3	15:00 to 17:59
3/Charger electric vehicle	1575	6	19:00 to 24:59
4/Dishwasher	800	3	10:00 to 12:59
5/Dishwasher	700	3	20:00 to 22:59
Water Pumping System	1755	2	10:00 to 11:00

The optimization process developed from the genetic algorithm will establish the best time for these loads to function, according to the minimum cost criterion given by hourly differentiated tariffs for these loads in the demand response program.

3. Energy management modeling

The micro-grid energy management problem has been addressed in recent publications. Nosratabi et al. [39] reviewed the concepts associated with the dispatch or generation programming and demand response in the micro-grid. Problems in programming the micro-grid resources are generally associated with factors such as the forecasting uncertainty of the input model variables, energy supply reliability, stability of the electrical system (frequency control, voltage, reactive power, etc.), emissions and final user prices. The models proposed in [40-43] have the common characteristic of the hierarchical arrangement of the power flux addressed from the sources to the loads, the storage systems or the grid. The computational organization is divided into special modules for input information management, forecasting, operation, optimization and finally the response module. The sum of the power inputs for each hour of day is used at a common link point.

The individual models of the different LabDER systems were integrated in a MATLAB© operating model of the hybrid generation-storage-demand system. This model calculates the hourly balance of the power from every source (photovoltaic, wind, hydrogen and biomass and grid), considering the required storage or the energy available (battery state of charge and level of the hydrogen tank) to meet the demand. The model considers internal consumption (electrolyzer stand-by energy consumption and leakage) and grid exports. Energy management considers dispatchable power generation (gasifier and fuel cell) and the opportunity of load time shift or even load disconnection as demand response.

The reference of the hourly power balance of the integrated system is the common AC single-phase bus. Inputs are the power from: photovoltaic array P_{PV}; wind turbine P_W ; gasifier generator P_{Gasif} ; fuel cell stack P_{FC} ; battery bank (when it discharges) $P_{BAT\text{-}disch}$; and grid power (when imported) $P_{Grid\text{-}in}$. The outputs include: electrolyzer consumption when producing hydrogen P_{ELY}; power required to charge the batteries $P_{BAT\text{-}ch}$,; export energy to the grid $P_{Grid\text{-}out}$; power consumption due to the stand-by of the all systems, control systems and air compressor to manage the hydrogen booster $P_{Loss+SC}$; and finally, power required by the residential loads P_{LOAD}. This balance does not consider the power from the backup system, since it is only used in emergencies. The balance is shown in Eq.(11).

$$\begin{aligned} &P_{PV} + P_W + P_{Gasif} + P_{FC} + P_{BAT-disch} + P_{Grid-in} = \\ &P_{ELY} + P_{BAT-ch} + P_{Grid-out} + P_{LOAD} + P_{LOSS+SC} \end{aligned} \tag{11}$$

To achieve this balance, the MATLAB operational model reads three types of data from Excel tables: *i.* master control data, which comprises operation modes, equipment parameters and maximum and minimum operation; *ii.* hourly data on temperature, irradiance, wind speed, load demand and consumer prices of energy from the forecasting system; *iii.* generation schedule of gasifier and fuel cell, plus the loads that can be disconnected or shifted over time from the demand response program. In addition to applying (1), the model must take into account the priorities of the resources used and the destination of this energy. Figure 9 shows the energy management strategy of the pre-scheduled controller by the XANTREX XW4548 Hybrid Inverter and SCADA system.

The controller must first check whether the energy from the photovoltaics, wind turbine and gasifier generator P_{WECS} is enough to supply the load demand P_{LOAD}, the minimum power of the electrolyzer P_{ELYMIN}, the minimum power to charge the batteries P_{BATMIN} and the minimum energy to keep the fuel cell P_{FCMIN} operating, as shown in Eq. (12).

$$P_{WECS} > P_{LOAD} + P_{ELYMIN} + P_{BATMIN} + P_{FCMIN} \tag{12}$$

As pre-scheduled, surplus energy is distributed in the following order: first, all the energy is used to charge the batteries; if batteries are fully charged (*SOCBAT* =100%), energy surplus will be used to produce hydrogen if the tank is not full. Maximum and minimum battery state of charge and hydrogen tank levels are strictly controlled. When all storage systems are full, the surplus energy is injected into the grid.

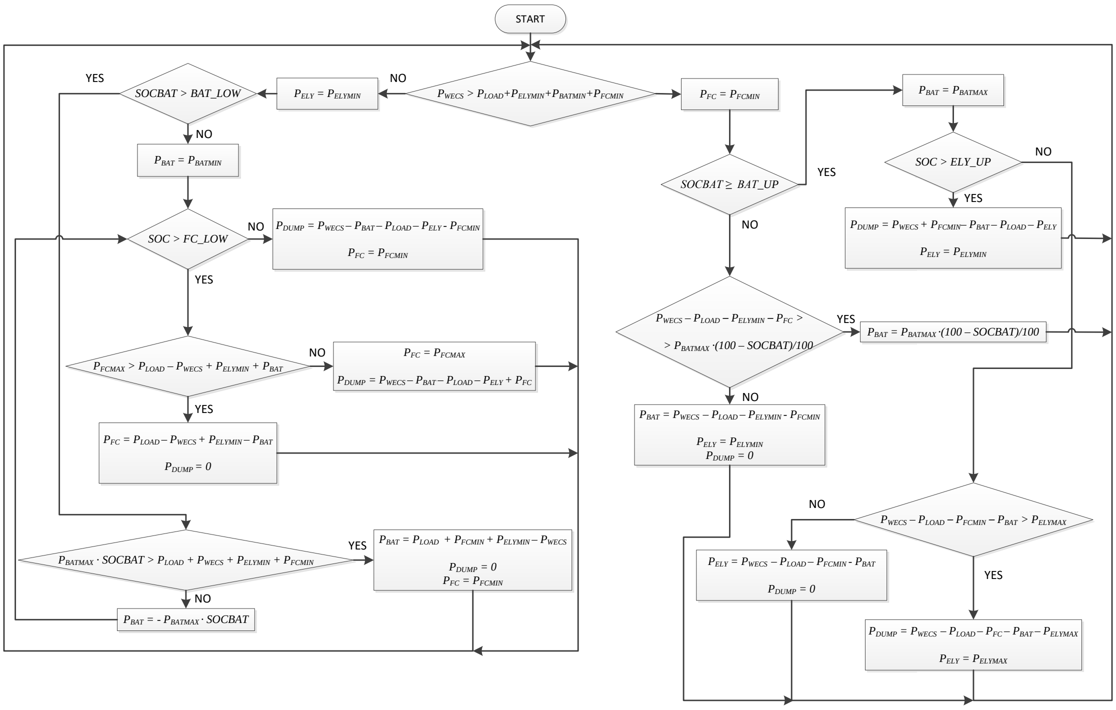

FIGURE 9 Energy management strategy of experimental micro-grid

When the conditions in Eq. (12) are not met it will be necessary to use stored energy. In this case the order is in reverse, with a FIFO system (First In, First Out). When demand is greater than battery capacity or the batteries are low (*SOCBAT* = 40%), the fuel cell will supply the required energy from hydrogen. This situation will continue till maximum fuel cell power is achieved or the hydrogen tank is at minimum (*SOCH2* = 10%). If batteries plus fuel cell cannot supply the load demand, energy will be taken from the grid. This hierarchy is based on the premise that batteries are considered a short-term storage element (due to the self-discharge coefficient) and hydrogen a long-term storage element (self-discharge coefficient zero).

There are two types of power generation in the proposed micro-grid operating model: non-dispatchable generation, depending on the availability of solar and wind resources, and dispatchable generation (FC and gasifier generator set), with the idea of satisfying the entire base load mainly from the gasifier. The nominal capacity of the gasifier is the largest of the LabDER's four generating systems.

As the gasifier system can reach maximum power (8000 W) from minimum (1600 W) in 10 seconds, this time is not considered in the balance. The gasifier must be in continuous operation (at the same power output) for a minimum of 2 hours. The maximum capacity of the pellet hopper is 96000 Wh, so that when the hopper must be refilled, the gasifier stops for one hour. Figure 10 shows the restrictions of the gasifier system in terms of the electrical power delivered to the common single-phase AC bus.

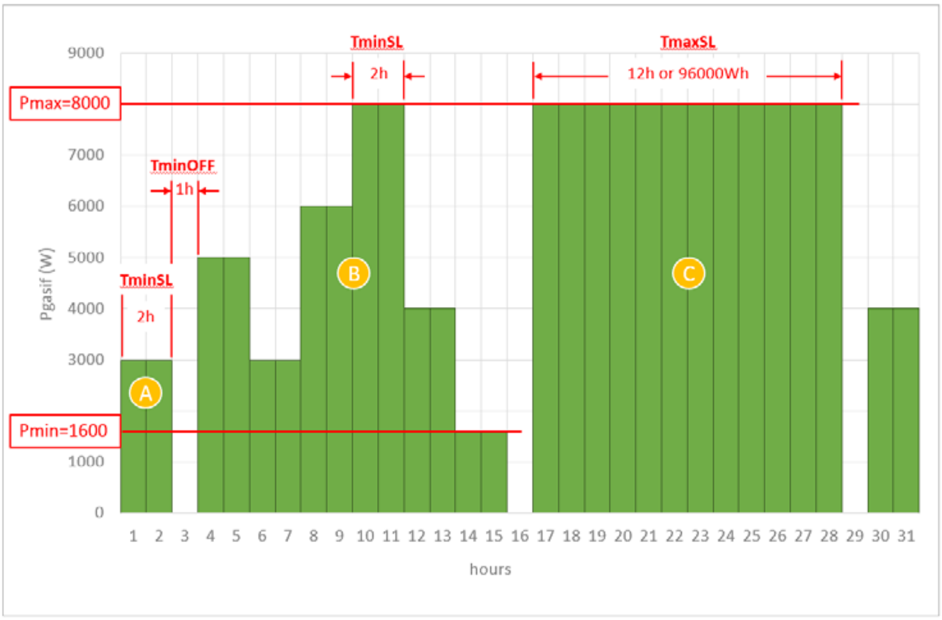

FIGURE 10 Rules of gasifier system operation: A, minimum time of operation in stable load (2 hours); B, variation according to the demand (maximum 96000 Wh) and 1 hour to refuel; C, maximum time at stable load in maximum power.

The operating model does not perform any optimization process in terms of the dispatch of the generating systems, it simply performs the hourly energy balance according to the order and rules described in Figure 9, delivering excess energy to the grid or requesting energy from it in the event of a deficit. Likewise, the 24-hour timing of the loads subject to the demand response program is initially based on typical household loads.

The micro-grid operating model starts from an initial dispatch from the gasifier and fuel cell, as well as from the daily timing of the loads subject to the demand response program. In this sense, the gasification system's operating strategy is to deliver the maximum possible power (8000 W) while complying with the maximum stable load operating time (*TmaxSL=12 hours*) and the rules given in Figure 10, since the gasification system is assumed to be at maximum efficiency.

In the case of the FC, the initial dispatch delivers 1100 W during 4 hours because of limitations of hydrogen production and storage. Initially, the FC starts its operation when the gasifier is out (Tminoff) and when there is a maximum demand during 2 consecutive hours. Table 5 shows the initial operation of the loads included in the demand response program. Figure 11 shows the energy balance on the common single-phase AC bus for 5 households on a summer day. The micro-grid operating model used was tested with hourly data of weather variables and hourly energy prices to the final consumer and base demand for the whole of 2016 in the city of Valencia (Spain). However, for purposes of analysis, only a portion of the data from the tests performed for the period from 13 to 27 June 2016 will be given here. This balance is specifically that of the ninth day (June 20), and it can be seen how each of the energy resources (bars in the figure) are used to cover the total demand (*Pload*) of five households, represented by the continuous red line. The initial location of the loads registered in the demand response program can be observed by means of the difference with the base demand (continuous blue line).

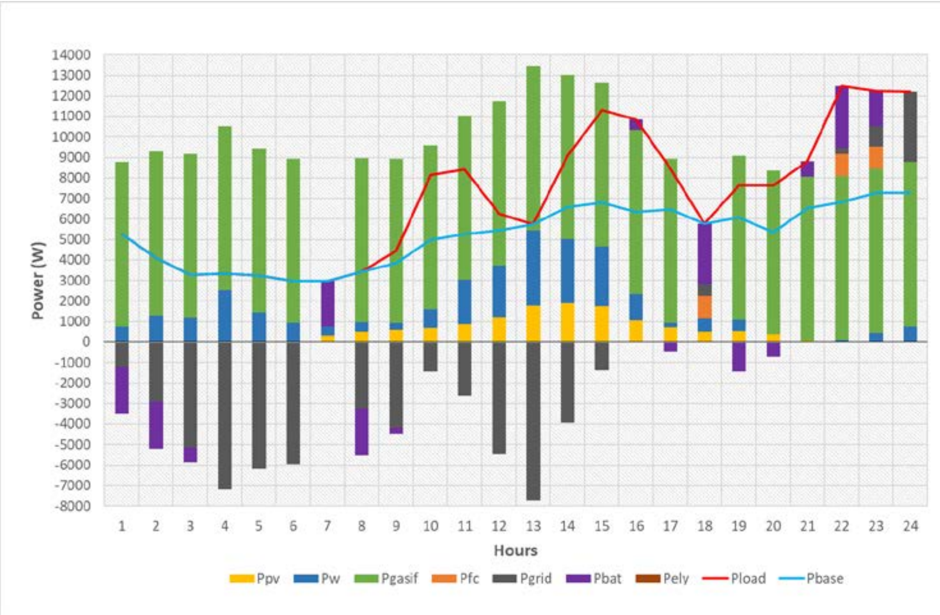

FIGURE 11 Results of the energy balance in the micro-grid operating model for the 5 households in a summer day case. Blue continuous line, base demand; red continuous line, dispatchable demand.

4. Algorithm description.

Sections 2 and 3 showed how the LabDER can be simulated to effectively represent its actual behavior. This simulator can be used as if it were a real micro-grid power generator connected to any system in order to test different high-level control strategies to optimize different indicators.

This study modeled a micro-grid supplying a residential unit composed of a series of houses with a configurable demand. The residential load can be configured with ***n*** houses whose base demand in per unit is shown in Figure 8.

Some of the loads can be scheduled to optimize grid performance. As the user knows the schedule a day in advance, he can take advantage of lower prices if he follows the proposed scheduling. The loads to be scheduled are: 600 W to 800 W for dishwashers, 2 kW to 2.5kW for swimming pool pumps, 1755W for the community water pump, or 1575 W to 3375 W to charge electric cars. Each load must be scheduled for a number of consecutive hours: 3 hours for dishwashers and pools, 2 hours for the community pump, and 4 to 6 for the chargers.

The micro-grid operator has to define a timetable for each of the detachable loads and send it to the consumers. Even though the controller can change the hourly inputs, the consumer should know the detachable loads at least a day in advance. The biomass power to be dispatched and the energy supplied to the electrolyzer to generate H_2 must also be defined. The controller plans a whole day and puts 24 values (for each input) into the system.

As the controller's main goal is to minimize operational cost of the system, its computation is a key issue. The total cost over the period analyzed for each of the energy sources is given by Eq.(13).

$$C_{SOURCE} = \sum_{h=1}^{t} Ps_h \cdot LCOEs \qquad (13)$$

Where, C_{SOURCE} is the total cost for t hours of the period analyzed, Ps_h is the power of source s at time h, and $LCOEs$ is the Levelized Cost of Electricity of source s. Table 2 shows the references used to define the LCOE of each energy source.

TABLE 2 LCOE Renewable sources value and reference

Source	**LCOEs [€/kWh]**	**Reference**
Photovolthaic	0.1578	Lazzard's Levelized Cost of Energy Analysis [44] - Minimum value for residential roof top: 187 $/MWh; 0,844 €/$)
Wind	0.08	Predescu, Economic Evaluation of Small Wind Turbines and Hybrid Systems For Residential Use [45]
Biomass	0.0962	Lazzard's Levelized Cost of Energy Analysis [44] – Maximum value for biomass direct: 114 $/MWh; 0,844 €/$)
Fuel Cell	0.0895	Lazzard's Levelized Cost of Energy Analysis [44] - Minimum value for FC: 106 $/MWh; 0,844 €/$)
Energy storage - Batteries	0.505	Lazzard's Levelized Cost of Energy Analysis [44] - Minimum value for residential lead acid batteries: 598 $/MWh; 0,844 €/$)

It is important to underline that the use of LCOE obtained in other works could be incorrect. The reason is that LCOE depends on the technology (affecting investment costs) and on its utilization in the site (affecting energy generation and operating costs). This work uses the reference values available in Lazzard's annual report [44] (with the exception of wind energy, since this report does not consider small-scale generation) in order to facilitate the comparison of results in subsequent works. This fact becomes a limitation to the operational model that could be solved with a LCOE calculation for each technology in each iteration of the controller, since the amount of energy generated by each technology is known at that moment. However, in the case of this work, the information of the Investment and Operation Costs is not available. Likewise, special care must be taken with the LCOE calculation of the batteries, since it depends significantly on the technology, number of duty cycles and other aspects of the working conditions associated with the location.

When calculating the total production cost of hydrogen C_{ELY}, and the cost of battery storage (in charge mode $C_{BAT\text{-}ch}$ for i hours), it should be remembered that these are fed from the photovoltaic, wind and gasifier systems. Likewise, when the batteries are discharged, the cost ($C_{BAT\text{-}disch}$ for j hours) is calculated from the battery $LCOE$, as in the equations (14)-(17).

$$C_{ELY} = \sum_{h=1}^{t} P_{ELY,h} \cdot LCOE_{WECS} \tag{14}$$

$$C_{BAT-ch} = -\sum_{i=1}^{t} P_{BAT,i} \cdot LCOE_{WECS} \tag{15}$$

$$C_{BAT-disch} = \sum_{j=1}^{t} P_{BAT,j} \cdot LCOE_{BAT} \tag{16}$$

$$LCOE_{WECS} = \frac{C_{FV} + C_{W} + C_{Gasif}}{\sum_{h=1}^{t} P_{PV,h} + \sum_{h=1}^{t} P_{W,h} + \sum_{h=1}^{t} P_{Gasif,h}} \tag{17}$$

Where P_{ELY} is the power consumed by the electrolyzer, P_{BAT} is the power from or to batteries, and $LCOE_{WECS}$ is the weighted average levelized cost of electricity from the renewable energy sources. Note that in battery charging a minus sign appears, since P_{BAT} is positive when the battery is delivering power. The Total Cost (*TCmg)* of meeting the demand from the experimental micro-grid is defined in Eq.(18) and the equivalent LCOE is as shown in Eq.(19).

$$\begin{aligned} TCmg &= C_{PV} + C_{W} + C_{Gasif} + C_{FC} + C_{BAT-disch} + C_{Grid} \\ &-(C_{ELY} + C_{BAT-ch} + I_{Grid}) \end{aligned} \tag{18}$$

$$LCOE_{EQ} = \frac{TCmg}{\sum_{h=1}^{t} P_{PLOAD,h}} \tag{19}$$

Where C_{PV}, C_{W}, C_{Gasif}, C_{FC} are the total costs of all sources, C_{Grid} is the total cost of purchasing power from the grid and I_{Grid} is the total income from power sales to the grid. In the former case, the energy purchase tariff T_P is used, which is defined hourly, while in the latter, income is calculated by means of a single agreed sales tariff T_S to the network, as in Eq.(20).

$$C_{Grid} = \sum_{h=1}^{t} P_{Grid-in,h} \cdot T_{P,h} \quad and, \quad I_{Grid} = \sum_{h=1}^{t} P_{Grid-out,h} \cdot T_{S} \tag{20}$$

Labder model simulates the operation of a full day (day *k*) and it needs to be fed with one hour sampled inputs. On one hand, the model needs prices, weather conditions and the base demand curve at each hour for the day to be simulated. On the other hand, the model needs to be fed with the hourly decisions on the fuel cell power and the biomass power to be dispatched and the scheduling of the disconnectable loads as they are defined on sections 2 and 3. Because of the simulation, the model generates two outputs: the global cost of the operation and the state of the storage systems (hydrogen and batteries).

In order to achieve the lowest cost, this paper proposes the use of a Model Predictive Controller (MPC) based on Evolutionary Algorithms (EA) to improve the overall cost of the operation. This controller is an optimizer that looks for the minimum cost controller to be implemented over a finite horizon. The control horizon is set to 7 days (one week). Figure 12 shows the control scheme.

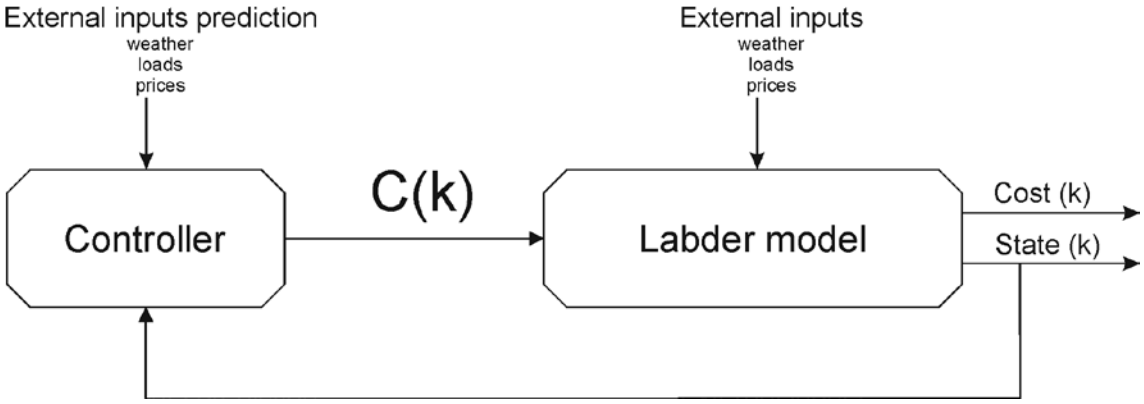

Figure 12. Control closed loop scheme.

The controller uses predictions on weather, prices and base demand curves, and the previous state of the system to compute the optimal distribution of power dispatching and disconnectable load configurations for the next day.

The optimal control command for day k is a $(a+2)\times 24$ matrix: $C_k = \{B_k, H_k, \overline{DL_k}\}$, where B_k (1×24) and H_k (1×24) are array including the 24 power dispatching values of biomass and hydrogen power, respectively. $\overline{DL}_k$ ($a\times 24$) is the matrix containing 24 hourly values of each of the n detachable load. This controller has to satisfy the restrictions stated in section 3 for each one of the power sources and the detachable loads.

In order to compute the optimal control command matrix, the controller searches for the set of seven consecutive control commands (for seven days) that achieve the minimum cumulative cost during this period. Therefore, controller dos not look for the best control command matrix for the next day but the best for the whole horizon of seven days. Then, the first day of the optimal control command matrix is selected as the control command for the next day. Thin kind of control is called MPC in the literature [21].

Therefore, the controller has to solve an optimization problem with restrictions. Because the model is very complex, this paper has chosen a heuristic optimization method based on evolutionary algorithms. This kind of optimization has been widely used to solve complex problems with restrictions [25]. The optimization methodology defines a set of candidates and tests each one to find the best under certain criteria. Once the best candidate has been found, the EA generates a new set of candidates based on the previous result. This new set is also tested so it is expected to improve the result of the previous generation. Some EA such as Particle Swarm Optimization (PSO) [22] have proven to converge to optimal solutions.

The EA implemented in this paper is based on the movement of a swarm known as PSO, which generates candidates in the population for testing. The algorithm creates variations in each control command to search for better solutions (lower cost solutions). Each of these control commands (including the best candidate of the last day) are simulated to find the best control strategy (P_{best}) in the population and the associated minimum cost. Figure 13 shows the flowchart of the optimization process.

The control computation starts by defining the first control command $C_{0,0} = \{B_{0,0}, H_{0,0}, \overline{DL}_{0,0}\}$, where $B_{0,0}$ stands for biomass power, $H_{0,0}$ is hydrogen power, and $\overline{DL}_{0,0}$ is the matrix containing the values of each detachable load. Each of these components includes 168 (7 days x 24 hours) hourly values to be simulated. This controller has to be simulated in Labbder and it is set as the best-computed solution. The first day of the simulation, this controller has to be defined externally. For the next day, the controller will use as the first control command the optimal controller of the previous day.

The next step (step 1) is performed by PSO, which generates a population (*P_1*) of m different controls $P_1 = \{C_{1,1}, \dots, C_{1,m}\}$

Each one of the controllers has the form:

$$C_{1,k} = \begin{bmatrix} cc_{1,1}^{\square} & \cdots & cc_{1,a+2}^{\square} \\ \vdots & \ddots & \vdots \\ cc_{1,168}^{\square} & \cdots & cc_{168,a+2}^{\square} \end{bmatrix} \tag{21}$$

Where $k \in [1,m]$, $[cc_{1,1}..cc_{1,168}]$ is the array including all biomass power values for the next week, $[cc_{2,1}..cc_{2,168}]$ is the array including all hydrogen power values for the next week and $[cc_{l,1}..cc_{l,168}]$ ($l \in [3,a+2]$ are the arrays including the next week power values of each detachable load. For the shake of generality, equation (21) uses a as the number of detachable loads.

Each one of the values is created from the best previous controller (the controller achieving the minimum cost). In the case of the first iteration, $C_{0,0}$ is used as the best controller because there is no previous result. So, each one of the values in equation (21) is computed as:

$$cc_{l,p}^{\square} = cc_{l,p}^{j-1} \cdot z \cdot q + cc_{l,p}^{j-1} \tag{22}$$

Where $l \in [1,168]$, $p \in [1,a+2]$, $cc_{l,p}^{j-1}$ is a corresponding value on the best previous controller, z) is a random number ($z \in [-1,1]$) and q is a perturbation (see [28]) that can be activated for some of the candidates in order to include perturbations in the swarm. In this work, half of the population is perturbed each 10 iterations with perturbations between [-2,2] thus kicking the candidates double far as the optimal solution. This strategy can avoid local minima [28].

Each candidate value is tested in order to find if they satisfy the restrictions. If not, values are adjusted to satisfy them. Then, each candidate in the population is tested so the controller ($\boldsymbol{C_{best,1}}$) achieving the minimum cost ($\boldsymbol{cost_{min,1}}$) is found.

The next step (step 2) is using a loop to look for the minimum. PSO generates a new population (P_2) from the $\boldsymbol{C_{best,1}}$ obtained in the previous iteration with equation (22) and each candidate is modified (if necessary) to fulfill the restrictions. Then, the whole population is tested in the Labder simulator, so the best controller in the population is found (the local best). If the cost of this controller ($\boldsymbol{C_{best,2}}$) is lower than the previous better cost ($\boldsymbol{cost_{min,1}}$), then the new overall best controller is set to $\boldsymbol{C_{best,2}}$. Else, no candidate improves the result of the previous generation, so the best controller is kept to be $\boldsymbol{C_{best,1}}$.

The next step consists of deciding if the algorithm continues testing new populations or if it has to stop. This paper implements two policies that can be activated or not if necessary as final conditions. The algorithm can be stopped if the number of iterations overpass certain value or if the improve in cost does not reaches a limit value (2% improve).

If the final condition is not met, then PSO generates a new population thus closing the loop (see Figure 13).

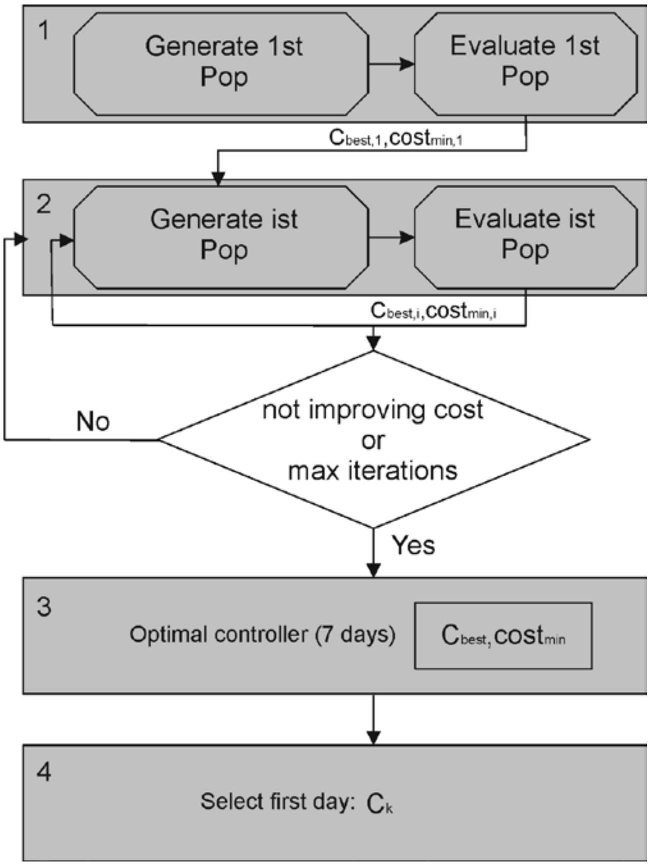

FIGURE 13 Controller computing diagram.

At the end of the optimization process (step 3), the controller has computed the values of the control commands that achieve the minimum cumulative cost (***$cost_{min}$***) for the next seven days (***C_{best}***).

The final controller command to be implemented (***C_k***) are the values corresponding to the first day (step 4).

5. Results and control performance.

The system was simulated with several configurations of the residential units in order to test the MPC controller. In the first scenario a residential unit of 3, 5, and 7 houses was tested with a pre-scheduled (non-optimized) controller (see Section 3). Figure 11 shows the initial energy balance for 5 households on a summer day, resulting in a mean total cost *TCmg* of 24.834 €/day and $LCOE_{EQ}$ of 0.147 €/kWh.

The same residential units were then controlled by the MPC controller to see whether it could improve on the pre-scheduled controller's results. The optimization EA was configured to generate 200 controllers in each iteration and a maximum of 100 iterations for each day. The system was tested for 15 days with 50 simulations for each scenario.

Figures 14 and 15 show how the MPC algorithm evolves the controller in order to reduce the cost. Figure 14 shows the initial situation with the pre-scheduled controller for the first 9 days. Since the control strategy remains constant, each detachable load is scheduled at the same time each day, so that *Pload* shows minor variations due to oscillations in *Pbase*. The renewable power generation *Pgen* remains stable each day, showing variations due to different weather conditions at constant biomass and fuel cell production. The system balances the overall energy, so that grid *Pgrid* and batteries *Pbat* absorb the surplus. Figure 15 shows the system controller under the MPC strategy. On the first day the system is controlled by the pre-scheduled controller. This controller is included as one of the candidates for the next day, together with the mutations proposed by the EA. The second day's system is controlled by the best controller achieved by the optimization process, which will also be one of the controllers to be tested for the third day. In a stable price and load scenario, the MPC algorithm therefore "polishes" the best candidate from the previous day in order to reduce the overall cost of the system.

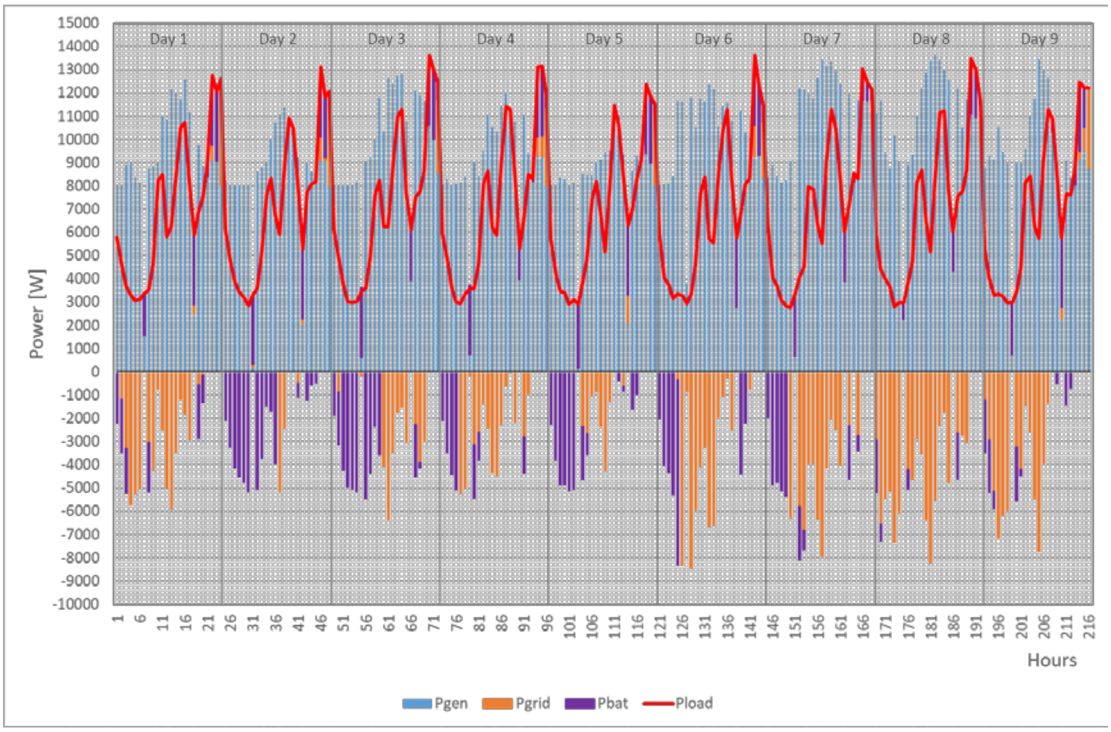

FIGURE 14 Hourly results in a week from a pre-scheduled controller for 5 households in summer days.

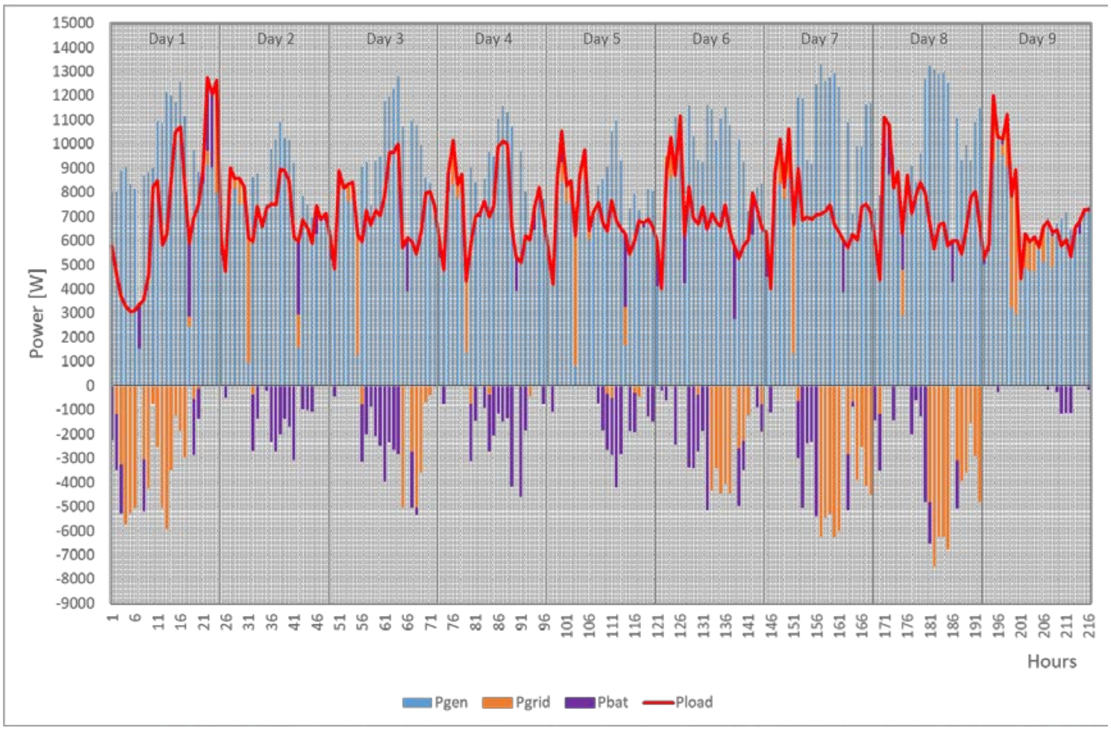

FIGURE 15 Weekly results from MPC controller for 5 households in summer days.

It can be seen that the demand curve *Pload* changes its shape by gradually moving the detachable loads to the cheapest hours of the day (also the hours with the lowest base demand) thus reducing the cost. The most refined controller (day 9) forces each detachable load to the first day times and optimizes biomass use. Figure 16 shows in detail the hourly behavior of the generation dispatch, the relocation of the transferable loads in the demand response program and the energy balance with the grid to satisfy the demand on day 9 (see Figure 11). Note that no hydrogen energy is used. There are two reasons for this behavior: firstly, the total energy generated is optimized and less energy needs to be stored. Secondly, the cost of storing energy as internal energy of hydrogen molecules is much higher than the cost of storing energy in batteries, due to the low power installed and the fact that the electrolyzer mostly works at partial load, reducing its efficiency, so that the algorithm discards hydrogen storage. Dispatchable demand is placed where the base demand is lowest and energy from the grid is cheapest.

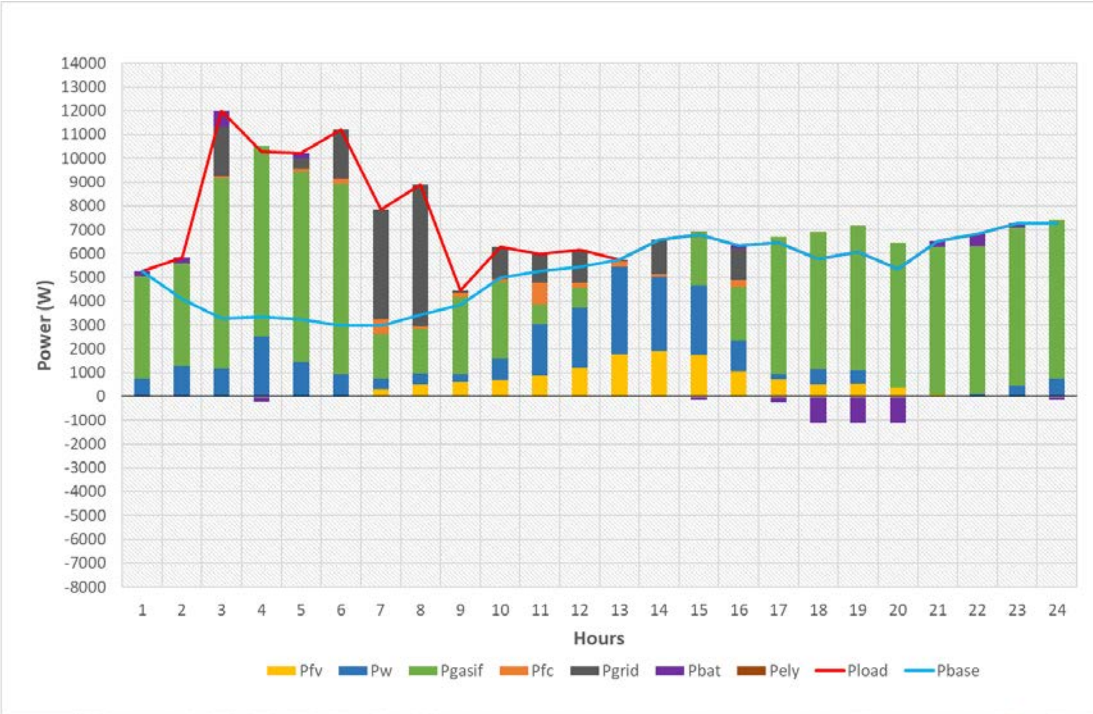

FIGURE 16 MPC results for 5 households on optimal summer day. Blue continuous line - base demand; red continuous line - dispatchable demand

Mean *TCmg* drops to 21.161 €/day and $LCOE_{EQ}$ to 0.123 €/kWh, with a 14.790% mean improvement in *TCmg* and 16.211% in the LCOE. *TCmg* and *LCOE* are improved in the 8% to 17% range, according to the number of houses involved. The standard deviation of the data remains at low values, indicating that there is no improvement on specific days, but over the whole period.

The EA performance in Figure 17 shows the evolution of *TCmg* for the best daily controller found during the optimization process (forcing 100 iterations for each day). The *TCmg* values are the sum of the seven best cost wise days. It can be seen that the optimizer sharply reduced the cost during the first 10 iterations, with a slight improvement up to iteration 20, after which the performance remained constant. When the controller checks a threshold in cost improvement (1%) in order to stop the process, the number of iterations oscillates between 8 and 10, thus reducing the computational cost. The average computing time of the MPC is 21.9 seconds, with an SD of 5.69 seconds (Windows® x64 Intel® Core® i5, 3GHz, 8GB RAM). This means it is suitable for computing a daily schedule without problems, while the short computation time shows that this system could also be used to configure hourly system outputs.

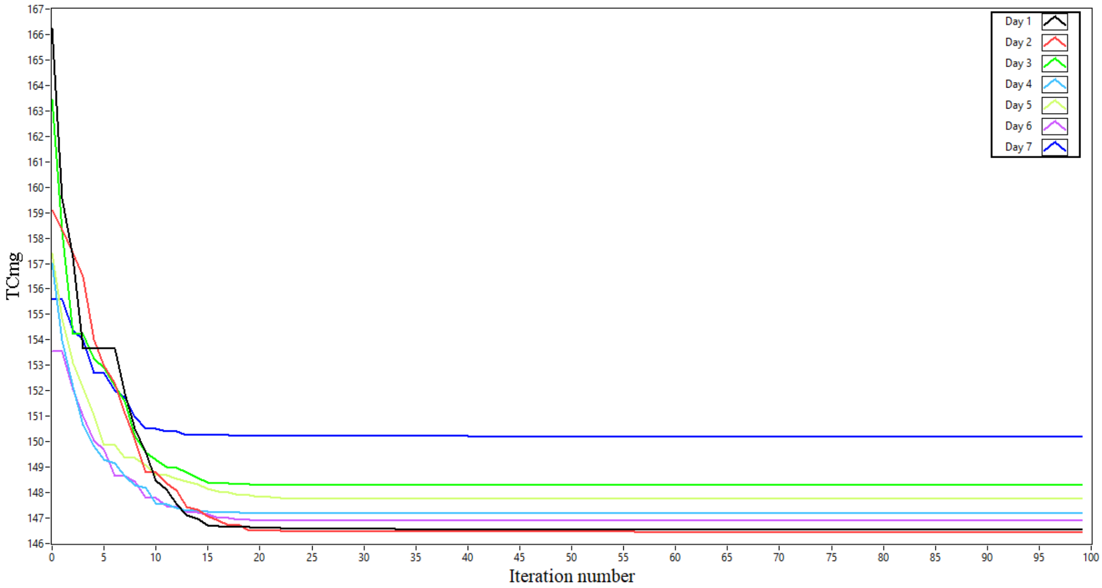

FIGURE 17 Total costs of micro-grid *TCmg* evolution during the optimization process.

6. Conclusions.

A control system was designed to optimize energy supply to a residential load from a hybrid renewable energy system connected to the public grid. The energy sources and storage systems studied were those installed in the LabDER experimental laboratory of the *Universitat Politècnica de València*. In order to check the controller's performance, a mathematical model was built from the experimental data collected in the laboratory from residential loads following a response demand program. The objective was for the controller to guarantee the supply of energy to the loads at the minimum cost according to the defined cost equations.

A Model Predictive Control Strategy based on Evolutionary Algorithms was developed, which searches for the minimum cost controller to be implemented over a finite horizon.

The simulation results obtained indicate that the MPC searches for a stable and smooth control strategy that improves the total cost of the system by defining the best time and power level to be generated by the biomass system and the PEM in relation to the expected values of the external inputs.

To demonstrate the improvements created by the MPC strategy actions, the initial control strategy (pre-scheduled controller) is set to operate the gasifier at maximum efficiency and use it the only dispatchable renewable source. The proposed controller achieved a 14.790% mean improvement in total micro-grid costs and 16.211% in LCOE, or even up to 17% in LCOE, according to the number of residential units considered.

Future studies are planned to deal with non-stable scenarios, including price changes due to international conditions, load changes, failures and other variations.

REFERENCES

1. Greenblat J, et al. The Future of Low-Carbon Electricity. Annual Review of Environment and Resources 2017;42:289-316
2. Yuan C, et al. Economic Power Capacity Design of Distributed Energy Resources for Reliable Community Microgrids. 9th International Conference on Applied Energy, ICAE2017, 21-24 August 2017, Cardiff, UK. Energy Procedia 2017;00:000–000
3. Chauhan A, Saini R. A review on integrated renewable energy system based power generation for stand-alone applications: configurations, storage options, sizing methodologies and control. Renewable and Sustainable Energy Reviews 2014;38:99–120.
4. Sinha S, Chandel S. Review of software tools for hybrid renewable energy systems. Renewable and Sustainable Energy Reviews 2014;32:192–205.
5. Bhandari B, et al. Optimization of hybrid renewable energy power systems: A review. International Journal of Precision Engineering and Manufacturing-green Technology 2015;2(1):99-112.
6. Shivarama K, Sathish K. A review on hybrid renewable energy systems. Renewable and Sustainable Energy Reviews 2015;52:907–916.
7. Hina A, Palanisamy K. Optimization in microgrids with hybrid energy systems – A review. Renewable and Sustainable Energy Reviews 2015;45:431–446.
8. Sinha S, Chandel S. Review of recent trends in optimization techniques for solar photovoltaic–wind based hybrid energy systems. Renewable and Sustainable Energy Reviews 2015;50:755–769.
9. Siddaiah R, Saini R. A review on planning, configurations, modeling and optimization techniques of hybrid renewable energy systems for off grid applications. Renewable and Sustainable Energy Reviews 2016;58:376–396.
10. Al-falahi M, Jayasinghe S, Enshaei H. A review on recent size optimization methodologies for standalone solar and wind hybrid renewable energy system. Energy Conversion and Management 2017;143:252–274.
11. Maleki A, Pourfayaz F. Optimal sizing of autonomous hybrid photovoltaic/wind/battery power system with LPSP technology by using evolutionary algorithms. Solar Energy 2015;115:471–483.
12. Hernández-Torres D, Urdaneta A, De Oliveira P. A hierarchical methodology for the integral net energy design of small-scale hybrid renewable energy systems. Renewable and Sustainable Energy Reviews 2015;52:100–110.
13. Baghaee H, Mirsalim M, Gharehpetian G. Multi-objective optimal power management and sizing of a reliable wind/PV microgrid with hydrogen energy storage using MOPSO. Journal of Intelligent & Fuzzy Systems 2017;32(3):1753-1773.
14. Cau G, Cocco D, Petrollese M, Knudsen S, Milan C. Energy management strategy based on short-term generation scheduling for a renewable microgrid using a hydrogen storage system. Energy Conversion and Management 2014;87:820–831.
15. Sharafi M, ElMekkawy T, Bibeau E. Optimal design of hybrid renewable energy systems in buildings with low to high renewable energy ratio. Renewable Energy 2015;83:1026-1042.
16. Wu Z, Tazvinga H, Xia X. Demand side management of photovoltaic-battery hybrid system. Applied Energy 2015;148:294–304.
17. Ranjbar M, Kouhi S. Sources’ Response for supplying energy of a residential load in the form of on-grid hybrid systems. Electrical Power & Energy Systems 2015;64:635-645.
18. Wang X, Palazoglu A, El-Farra N. Operational optimization and demand response of hybrid renewable energy systems. Applied Energy 2015;143:324–335.
19. Ren H, Wu Q, Gao W, and W. Zhou. Optimal operation of a grid-connected hybrid PV/fuel cell/battery energy system for residential applications. Energy 2016;113:702-712.
20. Dufo R, et al. Daily operation optimisation of hybrid stand-alone system by model predictive control considering ageing model. Energy Conversion and Management 2017;134:167–177.
21. F. Borrelli, A. Bemporad, M. Morari. Predictive Control for Linear and Hybrid Systems. Cambridge university Press. 2017
22. B.Y. Qu and Y.S. Zhu and Y.C. Jiao and M.Y. Wu and P.N. Suganthan and J.J. Liang. A survey on multi-objective evolutionary algorithms for the solution of the environmental/economic dispatch problems. Swarm and Evolutionary Computation. 38, pp 1 – 11. 2018

23. Habib Ullah, Subrata Paul, Jae-Do Park. Real-time electricity price forecasting for energy management in grid-tied MTDC microgrids. 10.1109/ECCE.2018.8557478.
24. Xun Wang. Model predictive control of a hybrid renewable energy system in an urban environment. Thesis project Biobased Chemistry and Technology. Wageningen University.
25. C. Segura, A, Hernandez-Aguirre, F. Luna, and, E, Alba. Improving Diversity in Evolutionary Algorithms: New Best Solutions for Frequency Assignment IEEE TRANSACTIONS ON EVOLUTIONARY COMPUTATION, VOL. 21, NO. 4, AUGUST 2017 539
26. Guo, L.; Meng, Z.; Sun, Y.; Wang, L. Parameter identification and sensitivity analysis of solar cell models with cat swarm optimization algorithm. Energy Convers. Manag. 2016, 108, 520–528
27. García-Triviño, P.; Gil-Mena, A.J.; Llorens-Iborra, F.; García-Vázquez, C.A.; Fernández-Ramírez, L.M.; Jurado, F. Power control based on particle swarm optimization of grid-connected inverter for hybrid renewable energy system. Energy Convers. Manag. 2015, 91, 83–92.
28. [Ariza] Ariza Chacón, H.E.; Banguero, E.; Correcher, A.; Pérez-Navarro, Á.; Morant, F. Modelling, Parameter Identification, and Experimental Validation of a Lead Acid Battery Bank Using Evolutionary Algorithms. Energies 2018, 11, 2361
29. Pérez-Navarro A, et al. Experimental verification of hybrid renewable systems as feasible energy sources. Renewable Energy 2016;86:384–391.
30. Abad B, Sánchez C, Alfonso D, Vargas C. TRNSYS model of the hybrid energy system in LabDER. 21st World Hydrogen Energy Conference, WHEC2016, 13–16 June 2016, Zaragoza, Spain.
31. Bellini A, Bifaretti S, Iacovone V, Cornaro C. Simplified Model of a Photovoltaic Module. IEEE Applied Electronics Conference, AE 2009, 9–10 September 2009, Pilsen, Czech Republic.
32. Hadj Arab A, Chenlo F, Benghanem M. Loss-of-load probability of photovoltaic water pumping systems. Solar Energy 2004;76:713–723.
33. Villalva M, Gazoli J, Filho E. Comprehensive approach to modeling and simulation of photovoltaic arrays. IEEE Transactions on Power Electronics 2009;24(5):1198–1208.
34. Lydia M, et al. A comprehensive review on wind turbine power curve modeling techniques. Renewable and Sustainable Energy Reviews 2014;30:452–460.
35. Vargas C. Estudio comparativo de la utilización de las tecnologías de gasificación Downdraft y lecho fluidizado burbujeante para la generación de energía eléctrica en aplicaciones de baja potencia. Doctoral dissertation. Universidad Politécnica de Valencia. Valencia; 2012.
36. Montuori L, Alcázar M, Álvarez C, Domijan A. Integration of renewable energy in microgrids coordinated with demand response resources: Economic evaluation of a biomass gasification plant by Homer Simulator. Applied Energy 2014;132:15–22
37. Mann R, et al. Development and application of a generalised steady-state electrochemical model for a PEM fuel cell. Journal of Power Sources 2000;86:173–180.
38. Shepherd C. Design of primary and secondary cells: II. An equation describing battery discharge. Journal of The Electrochemical Society 1965;112(7):657– 664.
39. Nosratabadi S, Hooshmand R, Gholipour E. A comprehensive review on microgrid and virtual power plant concepts employed for distributed energy resources scheduling in power systems. Renewable and Sustainable Energy Reviews 2017;67:341–363.
40. Sanseverino E, et al. An execution, monitoring and replanning approach for optimal energy management in microgrids. Energy 2011;36:3429–3436.
41. Mazidi M, Zakariazadeh A, Jadid S, Siano P. Integrated scheduling of renewable generation and demand response programs in a microgrid. Energy Conversion and Management 2014;86:1118–1127.
42. Vardakas J, Zorba N, Verikoukis C. A Survey on Demand Response Programs in Smart Grids: Pricing Methods and Optimization Algorithms. IEEE Communication Surveys & Tutorials 2015;17(1):152–178.
43. Nwulu N, Xia X. Optimal dispatch for a microgrid incorporating renewables and demand response. Renewable Energy 2017;101:16–28.
44. Lazard Ltd. Lazard's Levelized Cost of Energy Analysis – Version 11.0 https://www.lazard.com/media/450337/lazard-levelized-cost-of-energy-version-110.pdf
45. Predescu M. Economic evaluation of small wind turbines and hybrid systems for residential use. Renew. Energy Environ. Sustain. 2016;33(1): 1–6.

APPENDIX

Currents and Voltages in the photovoltaic model can be calculated as follows:

$$I_{SC} = I_{SCS}\frac{G}{G_S}[1+\alpha(T-T_S)] \tag{24}$$

$$V_{OC} = V_{SCS} + \beta(T-T_S) - \Delta V \tag{25}$$

$$I_{MPP} = I_{MPPS}\frac{G}{G_S}[1+\alpha(T-T_S)] \tag{26}$$

$$V_{MPP} = V_{MPPS} + \beta(T-T_S) - \Delta V \tag{27}$$

Where α and β are respectively the current and the voltage temperature coefficient. To improve the accuracy of the model, in the expressions (25) and (26) inserting a correction term, ΔV, taking into account voltage variation as a function of solar irradiance, which is calculated from the equation (28).

$$\Delta V = C_2 \cdot V_t \cdot m \cdot \ln(\frac{G}{G_S}) \tag{28}$$

Where V_t is the thermal voltage depending on the Boltzmann constant K_B, the temperature of the cell T and the electron charge q. Additionally, m is the diode quality factor.

$$V_t = \frac{K_B}{qT} \tag{29}$$

$$m = \frac{V_{MPP} + I_{MPP}\cdot R_0 - V_{OC}}{V_t\left[\ln\left(I_{SC} - \frac{V_{MPP}}{R_0} - I_{MPP}\right) - \ln\left(I_{SC} - \frac{V_{OC}}{R_0}\right) + \left(\frac{I_{MPP}}{I_{SC}\frac{V_{OC}}{R_0}}\right)\right]} \tag{30}$$

The internal resistance R_0 in the single diode model is calculated from the equation (31).

$$R_0 = \left(C_2\frac{V_{OC}}{I_{SC}(1+C_1)}\right) \tag{31}$$

Generating values for V_P from 0 to V_{OC}, at a given temperature and irradiance, the I_P current is obtained. The resistances R_S and R_P are then calculated from the reciprocal of the slope near to the open circuit point and that of the slope near to the short circuit point, respectively.

$$\left(\frac{dV}{dI}\right)_{V\approx V_{OC}} = -R_S \qquad \left(\frac{dV}{dI}\right)_{I\approx I_{SC}} = -R_P \tag{32}$$